ACS APPLIED MATERIALS & INTERFACES

Research Article

www.acsami.org

Water- and Humidity-Enhanced UV Detector by Using p-Type La-Doped ZnO Nanowires on Flexible Polyimide Substrate

Cheng-Liang Hsu,*[,†] Hsieh-Heng Li,[†] and Ting-Jen Hsueh*[,‡]

[†]Department of Electrical Engineering, National University of Tainan, Tainan 700, Taiwan, ROC

[‡]National Nano Device Laboratories, Tainan 741, Taiwan, ROC

ABSTRACT: High-density La-doped ZnO nanowires (NWs) were grown hydrothermally on flexible polyimide substrate. The length and diameter of the NWs were around 860 nm and 80−160 nm, respectively. All XRD peaks of the La-doped sample shift to a larger angle. The strong PL peak of the La-doped sample is 380 nm, which is close to the 3.3 eV ZnO bandgap. That PL dominated indicates that the La-doped sample has a great amount of oxygen vacancies. The lattice constants ~0.514 nm of the ZnO:La NW were smaller when measured by HR-TEM. The EDX spectrum determined that the La-doped sample contains approximately 1.27 at % La. The La-doped sample was found to be p-type by Hall Effect measurement. The dark current of the p-ZnO:La NWs decreased with increased relative humidity (RH), while the photocurrent of the p-ZnO:La nanowires increased with increased RH. The higher RH environment was improved that UV response performance. Based on the highest 98% RH, the photocurrent/dark current ratio was around 47.73. The UV response of water drops on the p-ZnO:La NWs was around 2 orders compared to 40% RH. In a water environment, the photocurrent/dark current ratio of p-ZnO:La NWs was 212.1, which is the maximum UV response.

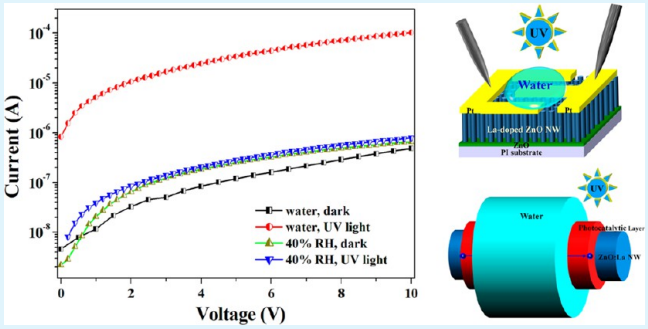

KEYWORDS: *ZnO nanowires, La-doped, PI, p-type, UV detector*

INTRODUCTION

Conventional metal oxide semiconductor photodetectors are based on materials such as tin oxide (SnO_2),[1] titanium dioxide (TiO_2),[2] zinc oxide (ZnO)[3] and indium oxide (In_2O_3).[4] Among them, ZnO is an n-type semiconductor with a large exciton binding energy of 60 meV, a high electron mobility of around 100 $cm^2 V^{-1} s^{-1}$, and a wide bandgap energy of 3.37 eV at room temperature. The ZnO nanostructure (NS) has received considerable scientific interest owing to their potential application in novel electrical, optical, magnetic and physical properties by large surface-to-volume ratio.[3,5−7] The morphologies of one-dimensional (1D) ZnO NSs include nanorods,[6] nanobelts,[8] nanorings,[8] nanofibers[9] and nanowires (NWs).[6,7] ZnO NWs can be synthesized by various methods, including chemical vapor deposition (CVD),[8,9] template-assisted growth,[10] catalyst-driven molecular-beam-epitaxy (MBE),[11] metalorganic chemical vapor deposition (MOCVD),[12] vapor−liquid−solid (VLS),[3] sol−gel systhesis,[13] and hydrothermal methods.[5,6] Of these synthesis techniques, CVD and hydrothermal synthesis are the most popular for ZnO NSs. The polyimide (PI) substrate can be formed into large-area substrates, flexible, lightweight and low-cost. A PI substrate has a high chemical resistance and excellent mechanical properties, which were used in passivation layer and insulating of semiconductor manufacturing. The hydrothermal method is better than other methods because the growth temperature 95 °C is very low, making the method suited to the chemical and physical properties of the flexible polyimide (PI) substrate and avoided Vicat softening point 225 °C of PI substrate. In this study, the p-ZnO:La NW photodetector is possible to integrate with semiconductor manufacturing by synthesis on PI passivation layer. Furthermore, the hydrothermal method has low cost and can be adopted in mass production.

Ultraviolet (UV) photodetectors (PDs) have various important potential applications, including space communication, flame detection, military and chemical applications. Over the past decade, many compact UV PDs have been prepared from p-n junctions and Schottky junction diodes with wide bandgap materials, such as SiCN,[14] diamond,[15] SiC,[16] III−V compounds,[17] and some II−V compounds.[8] ZnO NSs have great potential for use in UV PDs because of their high electron mobility, and good chemical and thermal stability.[3,18−22] The surface of ZnO NSs adsorb oxygen and plays an important role in UV photoresponse. The relative humidity (RH), temperature and reducing gas of the environmental conditions influence the adsorption of oxygen on the ZnO NSs surface. Up to now, there are some articles that have reported that the n-type ZnO UV photoresponse decreased with increasing RH.[21,22] The p-type ZnO has better photosponse stability in high RH, due to the physical characteristics of p-type

Received: August 14, 2013
Accepted: October 17, 2013
Published: October 17, 2013

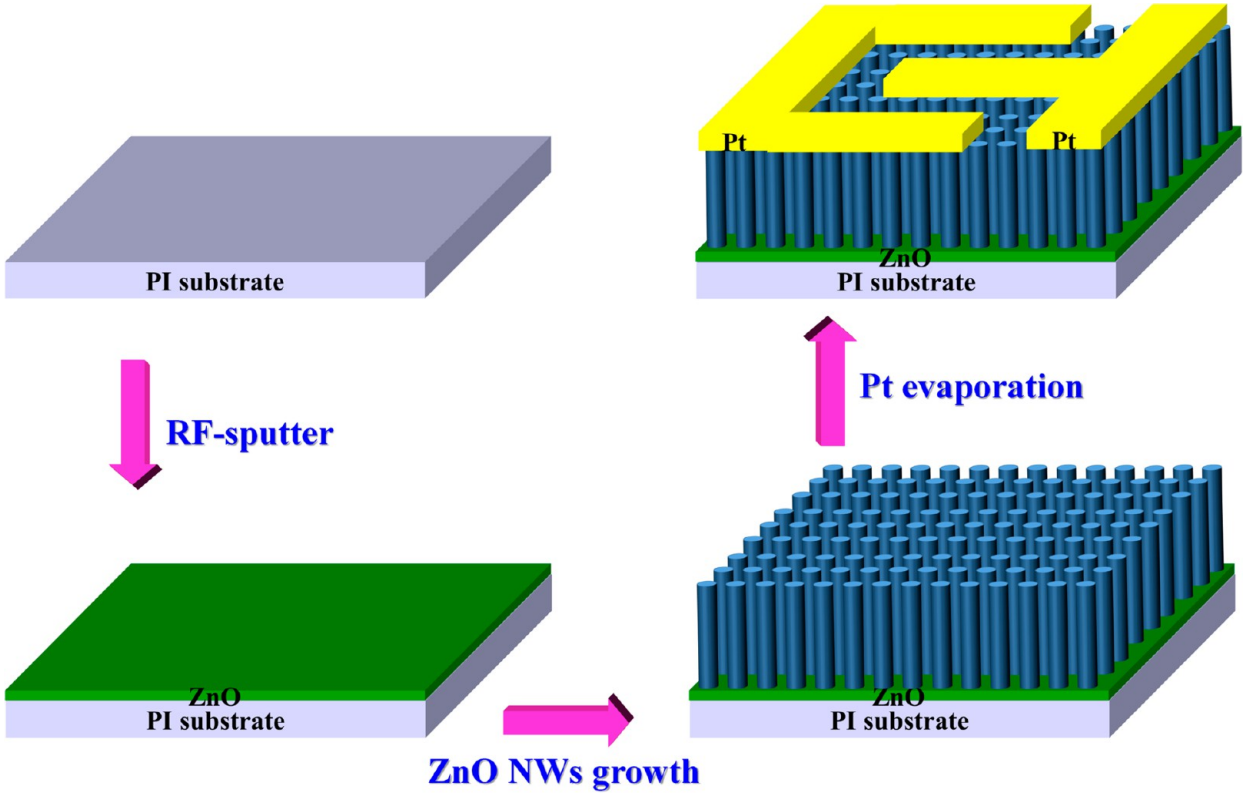

Figure 1. Schematic diagram of the growth and processing steps of ZnO:La NWs UV PDs.

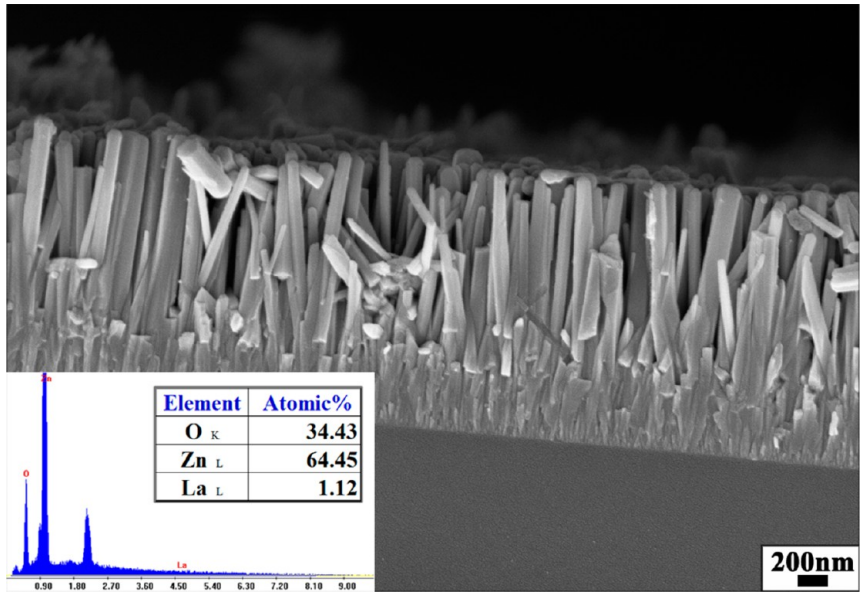

Figure 2. Cross-sectional FE-SEM images of ZnO:La NWs grown on ZnO/PI substrate. Inset at the bottom left corner shows the EDX spectra of the ZnO:La sample.

semiconductor being different than n-type.[23] Group-V (N, P, As, and Sb) atoms are well-known to be the most suitable dopants for p-type ZnO.[24−26] These p-type dopants substitute for oxygen. In recent times, rare earth metals (e.g., La, Eu, Dy, and Er) were doped into ZnO, which have been broadly researched and concentrated on luminescence properties.[27−29] Lanthanum (La) doped ZnO exhibits excellent photocatalytic and gas sensitivity.[27,28] In past reports, ZnO NSs with large surface-to-volume ratios should respond well to UV, and so this method can improve the performance of UV PDs. Up to now, a very small amount of literature has discussed that high humidity causes an enhanced p-type ZnO thin film photoresponse. The humidity and photoresponse properties of p-ZnO:La NWs has not been reported. In general, n-ZnO NSs showed increased decay with increasing humidity. In this study, the water and high humidity improve the UV photoresponse performance of p-type La-doped ZnO NWs. The La dopants improve the photocatalytic property of ZnO nanowires and enhanced

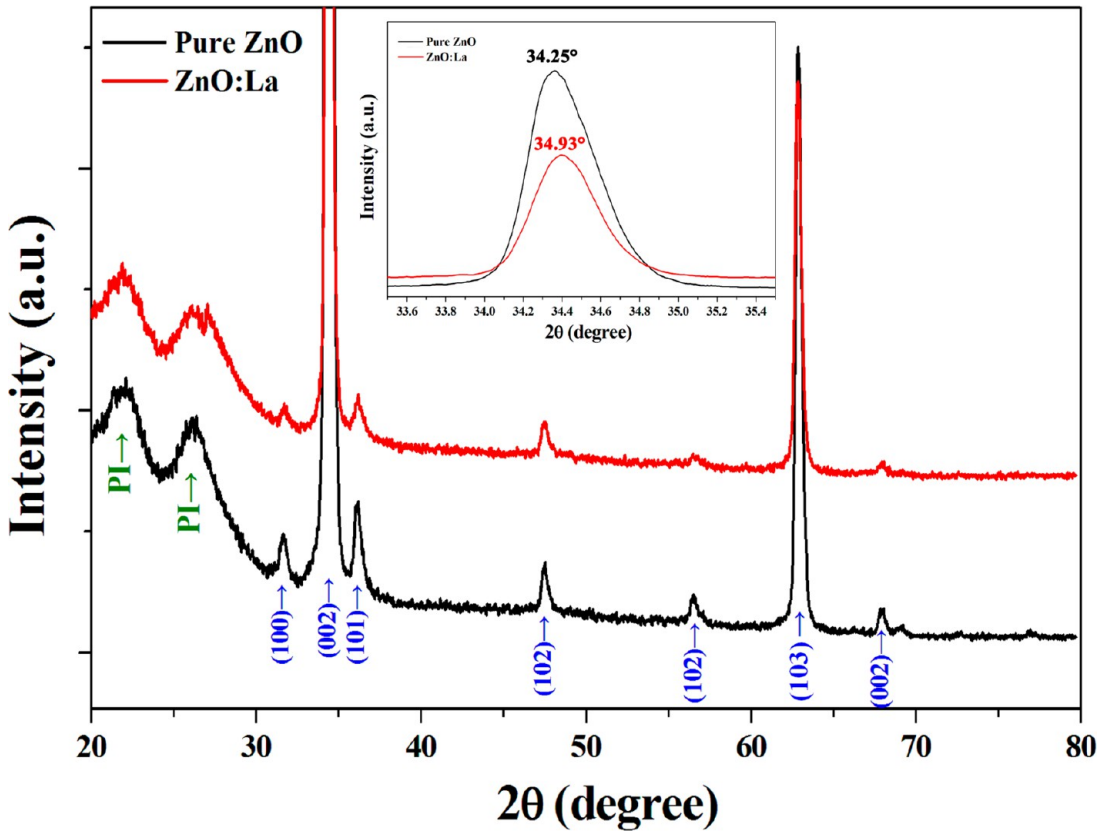

Figure 3. XRD 2θ scan spectra of the ZnO:La and ZnO NWs samples used in this study.

photoresponse in high humidity and water. In this investigation, the p-type UV PDs were fabricated by La-doped ZnO (ZnO:La) NWs and tested under UV illumination. The synthesis of p-type ZnO:La NWs was initiated on PI substrate by hydrothermal synthesis. The optical and electrical properties of the UV PDs are also discussed.

EXPERIMENTAL SECTION

Figure 1 schematically depicts the growth and processing steps utilized in this work. Before sputtering, the PI substrates were cleaned with ethanol and deionized (DI) water in an ultrasonic cleaner, and then baked at 100 °C for 10 min to remove moisture. ZnO seed layers were deposited on the PI using the RF magnetron sputtering method. The thickness of the ZnO film was approximately 30 nm. The ZnO nanowires were hydrothermally grown at 95 °C in a sealed beaker by immersing the PI substrates for 6 h in an aqueous solution of 0.08 M zinc nitrate hexhydrate [$Zn(NO_3)_2$], 0.06 M lanthanum nitrate hexahydrate [$La(NO_3)_3{\cdot}6H_2O$] and 0.08 M hexamethylenetetramine ($C_6H_{12}N_4$).

The $Zn(NO_3)_2$ and $La(NO_3)_3{\cdot}6H_2O$ were used as zinc and lanthanum resources. The $Zn(NO_3)_2/C_6H_{12}N_4$ molar ratio was always 1:1. Hexamethylenetetramine (HMTA) is a highly water-soluble, nonionic tetradentate cyclic tertiary amine. Thermal degradation of HMTA releases hydroxyl ions, which react with Zn^{2+} ions to form ZnO. UV PDs were then fabricated using a simple scheme. After the NWs growth, photolithography and liftoff were used to deposit Pt (99.999%) onto the electrode regions of the substrate.

The surface morphologies of the samples and size distribution of the NWs were characterized using a JEOL JSM-7000F field emission scanning electron microscope (FE-SEM) at 10 keV. Photoluminescence (PL) properties of these as-grown p-ZnO:La NWs were also characterized by a Jobin Yvon-Spex fluorolog-3 spectrophotometer. A Xe lamp emitting at 254 nm was used as the excitation source during PL measurements. The crystallography and structure of the as-grown NWs were characterized with a MAC MXP18 X-ray diffractometer (XRD) and a JEOL JEM-2100F high resolution transmission electron microscope (HR-TEM) operated at 200 kV. A picoammeter (Keithley 6487), connected via a GPIB controller to a computer, was used to measure the current−voltage ($I-V$) characteristics of the fabricated PDs. The $I-V$ characteristics were measured by sweeping the bias voltage from −10 to 10 V in the dark or under illumination at 365 nm. A hand-held UV lamp (wavelength = 365 nm) with a small power density of 0.25 mW/cm^2 was used as an excitation source during photocurrent measurements.

RESULTS AND DISCUSSION

Figure 2 displays the cross-sectional FE-SEM images of the ZnO:La NWs grown on ZnO/PI substrate. The images reveal that high-density NWs grew uniformly in the samples. As shown in Figure 2, the length and diameter of the ZnO:La NWs were around 860 nm and 80−160 nm, respectively. The inset image shows the energy-dispersive X-ray (EDX) spectrum of the La-doped sample, indicating that these NWs consist of Zn, O, and La. The La content of the NWs can also be estimated from the intensity ratios among the Zn, O and La peaks. The La contents of the samples is 1.12 atomic%. Figure 3 illustrates the XRD $\theta/2\theta$-scan spectra of the ZnO:La NWs and pure ZnO NWs samples, which demonstrate the crystallographic characteristics of the ZnO:La NWs and PI substrate. The pure ZnO NWs were prepared under the exact same conditions. The PI substrate yielded two peaks at around 22.54 and 26.13°. The (002) peak is much more intense than the other peaks, which indicates that the NWs have a preferential growth with the c-axis. Figure 3 reveals that all peaks of the La-doped sample shift to a larger angle as observed by the notable (002), (101), (102) and (103) peaks. Figure 3's inset image shows that the ZnO:La and pure ZnO NWs yielded a strong

(002) peak at 34.93 and 34.25°, respectively. The (002) peaks of the ZnO:La NWs is shifted by about 0.68°. In this study, the lattice constants a and c of the hexagonal wurtzite ZnO structure was evaluated from the (100) and (002) planes, respectively. The Miller indices were calculated by the following relation

$$\frac{1}{d^2_{(hkl)}} = \frac{4}{3}\left(\frac{h^2 + hk + k^2}{a^2}\right) + \frac{l^2}{c^2}$$

where d_{hkl} denotes the lattice spacing of the (hkl) plane, and a and c denote lattice parameters. The (100) and (200) were orientated at 2θ = 31.7 and 34.34°, respectively. The pure ZnO lattice constants a and c were determined as a = 3.259 Å and c = 5.222 Å. The ionic radius of the La^{3+} = 1.16 Å is larger than the Zn^{2+} = 0.74 Å. The La^{3+} ion is difficult to substitute the Zn^{2+} ion with Hume−Rothery rules, owing to the ionic radius of La^{3+} being larger than that of Zn^{2+} by about 56%. The La^{3+} ions prefer the interstitial position in the ZnO lattice where they form a complex with the surface oxygen vacancies of the ZnO NWs, and cause a decrease of the lattice parameters for the prepared ZnO:La ZnO NW. Suggest that decrease the crystalline lattice of the ZnO:La NWs is similar past report and attributed to the formation of La−O−Zn on the surface of ZnO:La NWs.[27]

Figure 4 shows the room-temperature PL spectrum of the ZnO:La NWs and ZnO NWs grown on ZnO/PI substrates.

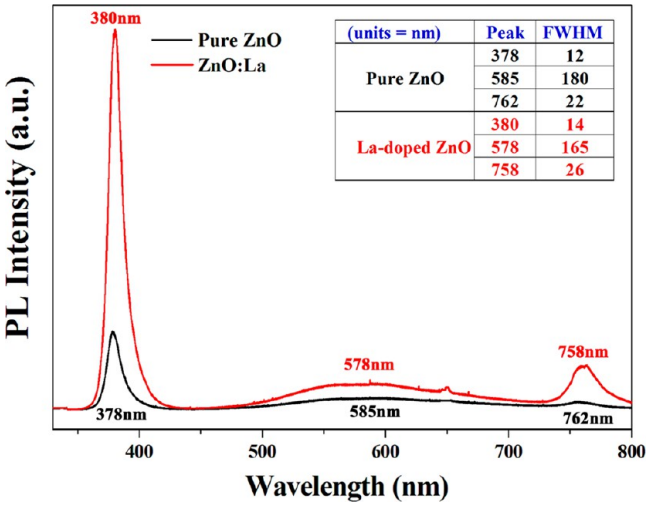

Figure 4. Room-temperature PL spectra of ZnO:La and ZnO NWs samples.

The ZnO:La NWs have a very high PL intensity in comparison to the pure ZnO NWs. The figure clearly shows strong peaks at about 380 nm and 378 nm with full widths at the half maxima (fwhm) of 14 and 12 nm, respectively. The ZnO:La NWs and ZnO NWs samples both undergo transitions close to the 3.3 eV ZnO band gap. Therefore, the two corresponding PL peaks are attributable to the recombination of free excitons through exciton−exciton collision.[30] Also, PL peaks of the ZnO:La NWs and ZnO NWs were observed, along with strong and broad bands at 578−585 and 758−762 nm. The green and red emission band around 2.14 eV (580 nm) and 1.63 eV (760 nm) originate from the oxygen vacancies and La impurities.[27,28] The 758 nm/380 nm peak ratio ~0.118 of ZnO:La NWs is higher than the 762 nm/378 nm peak ratio ~0.078 of ZnO NWs. This indicates that ZnO:La NWs have a great amount of oxygen vacancies due to the La impurities. The oxygen vacancies and La impurities would induce the formation of new energy levels in the bandgap. Hence, emission results from the radiative recombination of a photoexcited hole with an electron that occupies the oxygen vacancy and deep levels of the La impurity.

Figure 5a shows HR-TEM images of the top of the ZnO:La NW sample. The ZnO:La NW consists of structurally uniform

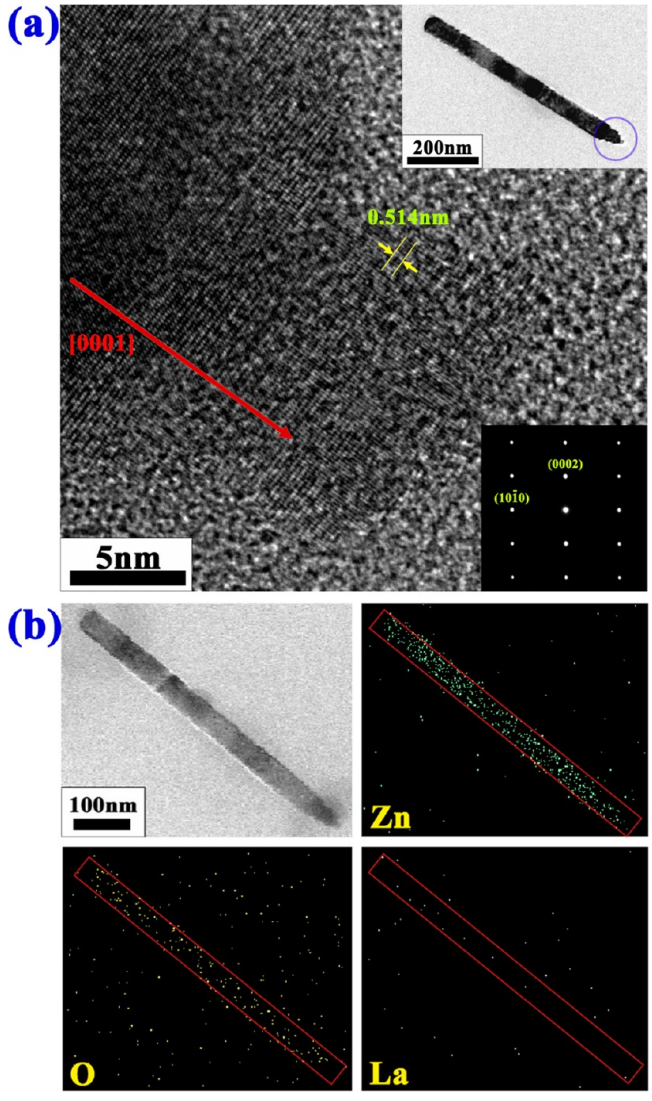

Figure 5. (a) HR-TEM images of the ZnO:La NW. The insets show the TEM image and corresponding SAED pattern of the NW; (b) TEM image and corresponding O, Zn, and La EDX spectroscopic mapping images, respectively.

single crystals with a wurtzite structure. ZnO:La NWs dispersions in liquid ethanol were prepared by the application of ultrasonic energy. Sonication is the most commonly used method for preparing finely dispersed ZnO:La NWs TEM samples, and it was utilized herein in the HR-TEM analysis and EDX mapping. The ZnO:La NWs were put into carbon paste using an ethanol carrier and the evaporation of ethanol. According to the HRTEM images, the crystal lattices are clearly well oriented with no observable defects. The 0.514 nm lattice spacing, observed from the figures, is associated with the ZnO (002) crystal plane. The ZnO lattice constant of 0.522 nm is

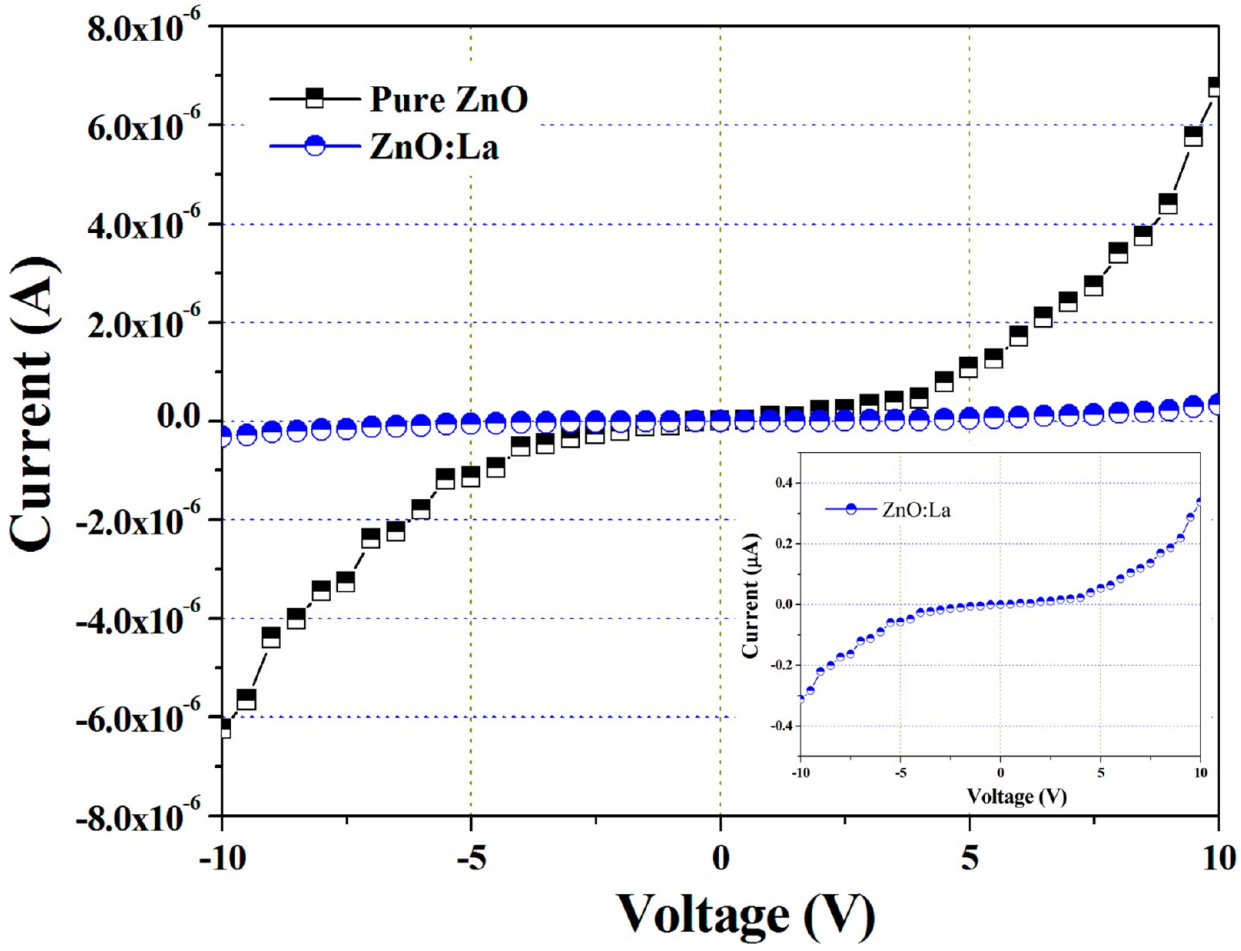

Figure 6. *I*−*V* characteristics of the ZnO:La NW PDs measured in the dark.

larger than that of ZnO:La NW at 0.514 nm because of the La impurity causing oxygen vacancies to increase and the lattice spacing to decrease. The upper left-hand portion of Figure 5a presents the TEM image of the ZnO:La NW. The depicted blue circle is zoom out HR-TEM image. In the bottom right-hand portion of Figure 5a, the SAED pattern indicates that the ZnO:La NWs are single crystals with a wurtzite structure, which is consistent with the XRD measurements. Figure 5b shows the TEM image and the corresponding Zn, O, La energy-dispersive X-ray (EDX) spectroscopic mapping images of the ZnO:La NWs. The mapping images demonstrate that high concentrations of Zn and O atoms are uniformly distributed throughout the NW. The ZnO NW contains approximately 1.27 at % La, as determined from the EDX spectrum. In contrast, the EDX mapping image of the La atoms reveals only a few spots because the La content is close to the detection limit of the proposed system. However, this image reveals that most La atoms are located in the region of the NW.

Based on the Hall Effect measurement, the determined ZnO:La NWs were p-type, sheet resistance = 29.37Ω/sq, Hall mobility = 11.1 $cm^2/(V\ s)$ and hole concentration (p) = 1.92×10^{16} cm^{-3} was low, because ZnO was natively n-type and difficult to turn into p-type. The pure ZnO NWs are n-type, have a sheet resistance = 13.99 Ω/sq, Hall mobility = 11.6 $cm^2/(V\ s)$, and electron concentration (e) = -3.85×10^{16} cm^{-3}. The La acts as a doping impurity, which reduces the electron concentration and increases hole concentration in the ZnO NWs. Figure 6 plots the *I*−*V* characteristics between the two neighboring electrodes that are bridged by ZnO NWs or ZnO:La NWs in the ambient atmosphere at room temperature. The measured current increased nonlinearly with the applied bias in the dark. The nonlinear increase confirmed the favorable Schottky barrier between the NWs and the electrodes. In general, the metal−semiconductor junctions form a rectifying Schottky barrier. These samples have not undergone the annealing process to eliminate Schottky rectifying characteristics and form ohmic contact. Hence, the *I*−*V* characteristic of PD in a dark environment is similar to that of a normal rectifying diode. The Schottky PD provides additional capabilities over other forms of PD in terms of speed and long wavelength detection capability. When a bias of 10 V was applied, the measured currents in the ZnO:La NWs and ZnO NWs were only 3.38×10^{-7} and 6.76×10^{-6} A, respectively. The latter was about 20 times the former. The likely explanation is that the La dopant increased the resistance, which is consistent with the Hall sheet resistance measurement results.

Figure 7a presents that *I*−*V* characteristics of the ZnO:La sample measured in the dark at 25 °C with various RH. The dark current of the ZnO:La sample decreased with increased RH. The value of dark current at a 10 V bias changed from 3.04×10^{-7} to 9.72×10^{-8} A when the RH in the chamber varied from 40 to 98%. Figure 7b depicts the RH responses of the ZnO:La sample with a 10 V applied bias. The RH responses of the device are defined as $[(I_{\text{various RH}} - I_{\text{RH=40\%}})/I_{\text{RH=40\%}}]$, where $I_{\text{various RH}}$ is the measured current in the dark at each RH

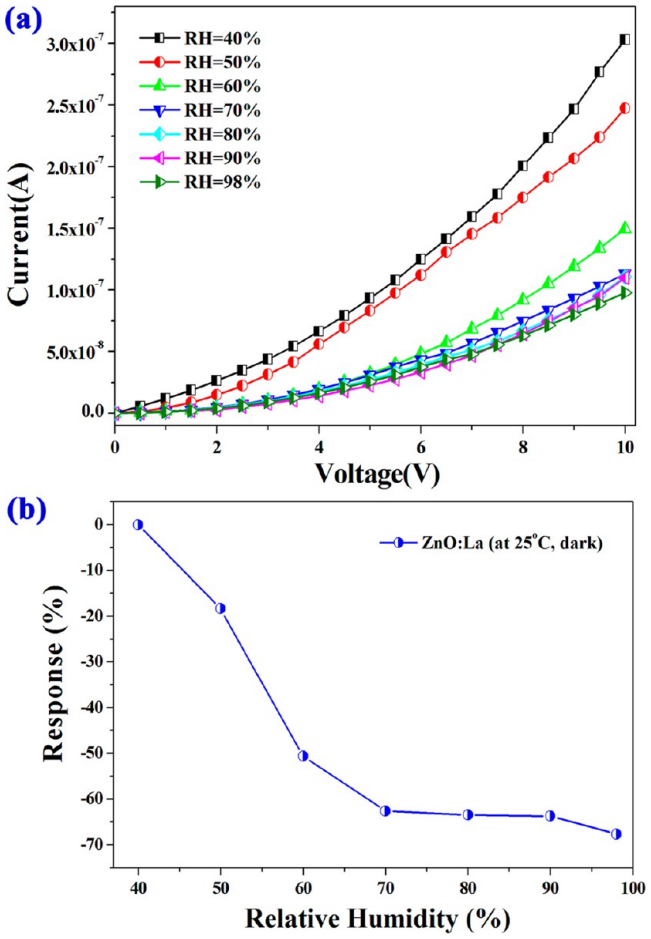

Figure 7. (a) $I-V$ characteristics of the ZnO:La sample measured in the dark with various RH; (b) RH responses of the ZnO:La sample with a 10 V applied bias.

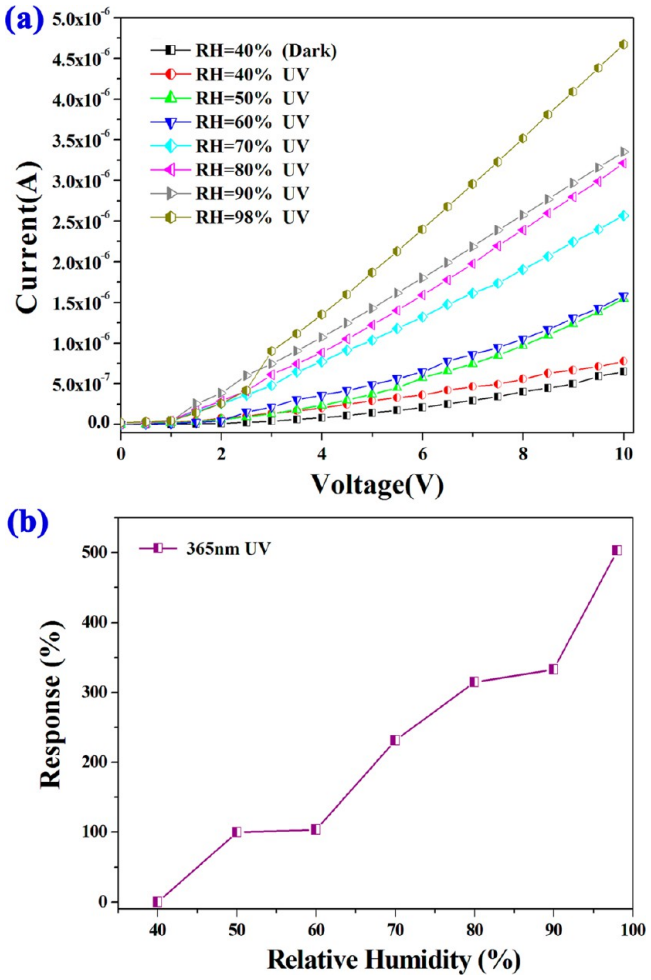

Figure 8. (a) $I-V$ characteristics of ZnO:La sample measured under UV with various RH. (b) RH responses of the ZnO:La sample with a 10 V applied bias under UV exposure.

condition, and $I_{RH=40\%}$ is the dark current at 40% RH. The response decreased quickly at less than 70% RH. When RH was increased to more than 70%, the response decreased gradually. The maximum response of −68% was observed at 98% RH due to the high humidity and slight water vapor impact.

Figure 8a shows the $I-V$ characteristics of the ZnO:La sample measured under UV illumination (365 nm) at 25 °C with various RH. The photocurrent of the ZnO:La sample increased with increased RH. The photocurrent value at 10 V bias changed from 7.85×10^{-7} to 4.68×10^{-6}A when the RH varied from 40% to 98%. All $I-V$ curves were close to linear, which differs from the dark $I-V$ curves, as shown in Figure 7(a). This suggests that UV light generated an amount of electron−hole pairs to reduce the Schottky barrier. Figure 8b displays the RH responses of the ZnO:La sample with a 10 V applied bias under UV exposure. The RH responses of the ZnO:La sample are defined by the same equation $[(I_{\text{various RH}} - I_{RH=40\%})/I_{RH=40\%}]$. The response increased quickly and was close to being a linear curve with increased RH. A linear fitting of the response curve has been established and the goodness of fit (R^2) was equal to 0.951. The 98% RH obtained the highest response, of around 500%. According to past reports, the UV photoresponse of ZnO NSs was decay around 10 times at high RH (~95%) in comparison with the 40% RH photoresponse.[21,22]

Figure 9 reveals the UV photocurrent (I_{UV}) to dark current (I_{Dark}) contrast ratio with various RH values. The I_{UV}/I_{Dark} ratio

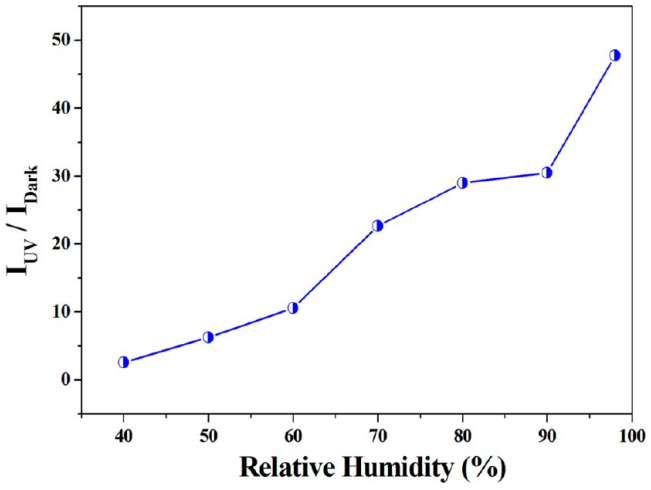

Figure 9. UV photocurrent (I_{UV}) to dark current (I_{dark}) ratio with various RH.

increased with increased RH. The highest I_{UV}/I_{Dark} ratio was around 47.73 at 98% RH, whereas the lowest I_{UV}/I_{Dark} ratio was only 2.56 at 40% RH. Although 40% RH is the general PD measurement atmosphere condition, the I_{UV}/I_{Dark} ratio of 2.56 is lower than past reports.[21,22] This suggest that La impurities

and the amount of oxygen vacancies reduce the ZnO:La NWs photocurrent to cause the lower ratio at 40% RH.

The sensing mechanism of gas-sensing semiconductors operates only at the surface. ZnO NWs are used in gas sensing, owing to their large surface-to-volume ratio. According to Barsan et al.,[31] interaction with atmospheric oxygen causes the ionosorption of molecular O_2^- and atomic (O^-, O^2) species at temperatures of 25−500 °C. At room temperatures, nearly all of the adsorbed atmospheric oxygen in their investigation was molecular O_2^-. The reaction kinetics are as follows[32]

$$O_2(\text{gas}) \leftrightarrows O_2(\text{ads})$$

$$O_2(\text{ads.}) + e^- \leftrightarrows O_2^-$$

Panels a and b in Figure 10 schematically depict that adsorption of O_2^- and water molecules at the surface of the p-ZnO:La and n-ZnO NWs at low RH and high RH, respectively. The surfaces of the p-ZnO:La and n-ZnO NWs have large quantities of O_2^- molecules and few water molecules at low RH, as shown in Figure 10a. Oxygen ionosorption receives free electrons from the surface of the p-ZnO:La and n-ZnO NWs. The conductivity of the p-ZnO:La NW was increased because of the hole concentration increase in the NW surface by the disappearance of electrons. Accordingly, a depletion layer with low conductivity is formed near the surface of the n-ZnO NW. This process also leads to the upward band bending near the surface. The adsorption of O_2^- molecules significantly increases p-ZnO:La and decreases n-ZnO conductivity, because of the NW large surface-to-volume ratio. Figure 10(b) reveals that water molecules may replace the O_2^- molecules and released electrons from the O_2^- molecules at high RH [$2H_2O(\text{ads.}) + O_2^-(\text{ads.}) \rightarrow 2H_2O_2 + e^-$].[21] The released electrons reduced the hole concentration of the p-ZnO:La NW surface, which then decreased the conductivity of the p-ZnO:La NWs. The conductivity of the n-ZnO NWs was increased with considerable release of electrons, whereas its depletion layer partially disappeared.

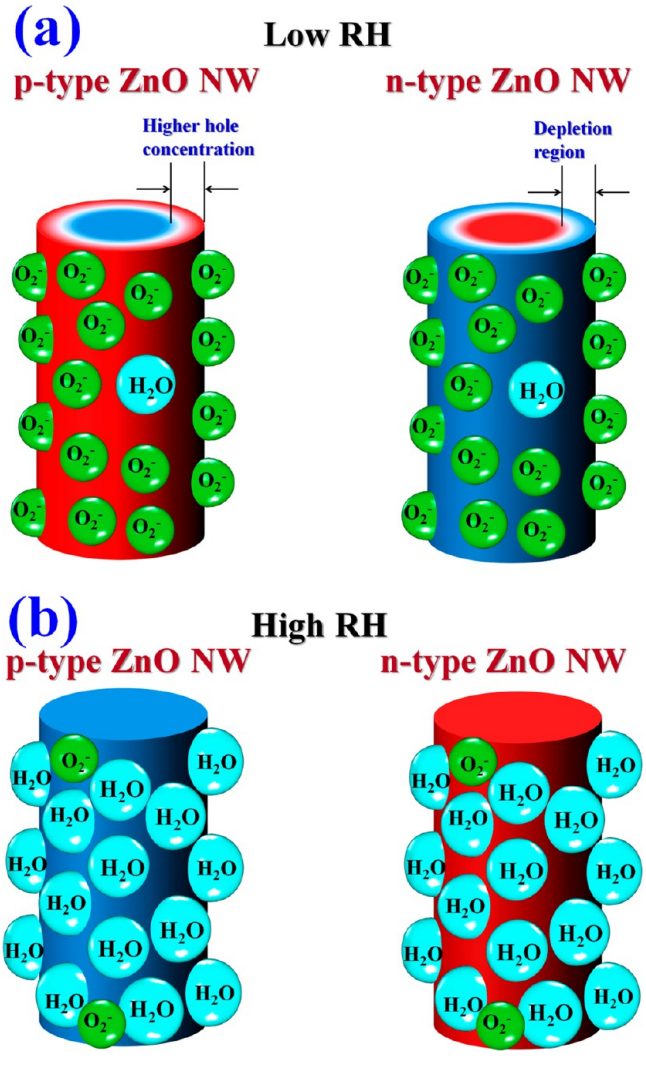

Figure 10. Schematic of the adsorption of O_2^- and water molecules at the surface of the p-type ZnO:La and n-type ZnO NWs at (a) low RH; and, (b) high RH.

Panels a and b in Figure 11 show schematics of UV exposure on the p-ZnO:La and n-ZnO NW surfaces at low and high RH, respectively. UV light absorption generates electron−hole pairs on the surface of the NWs. Figure 11a reveals that these samples were placed in a low RH environment with UV exposure. The photogenerated holes oxidize the adsorbed negatively charged oxygen ions on the surface [$O_2^-(\text{ads.}) + h^+$

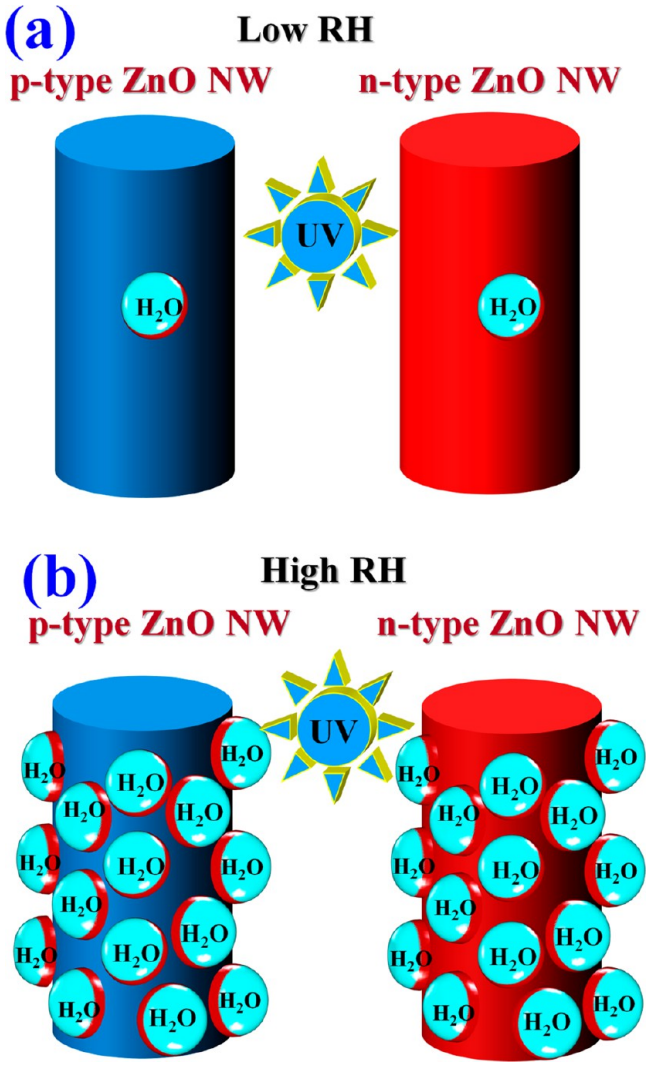

Figure 11. Schematic of UV exposure on the p-type ZnO:La and n-type ZnO NW surfaces at (a) low RH; and, (b) high RH.

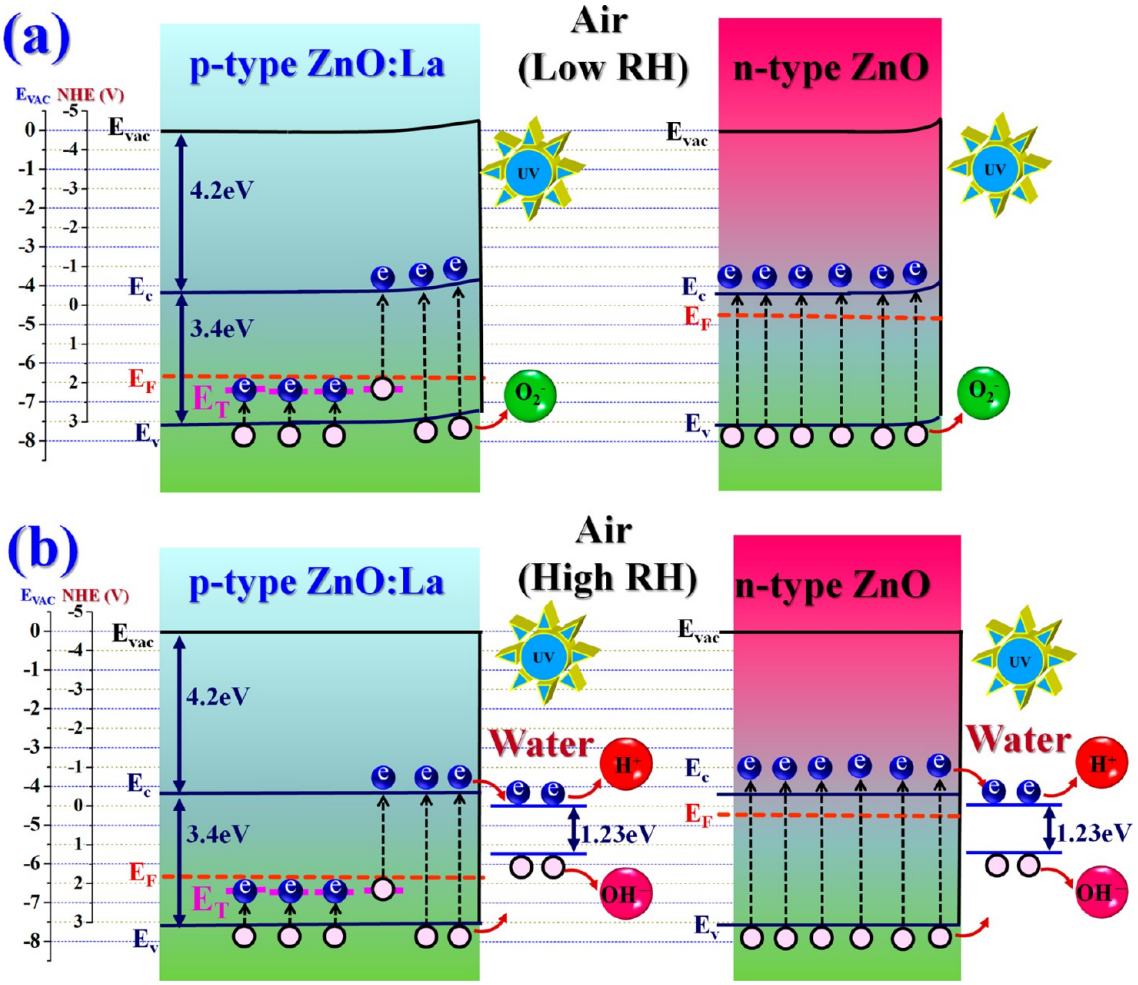

Figure 12. Schematic of the band diagrams band edge positions (vs vacuum and NHE) of the p-type ZnO:La and n-ZnO NWs with UV exposure at (a) low RH; and, (b) high RH.

→ O_2(gas)], whereas the remaining electrons decreased the hole concentration of the p-ZnO:La NW surface. Although the UV photo generates large amounts of electron−hole pairs to increase conductivity, the holes of the p-ZnO:La NW surface were partially reduced to slightly decrease the photocurrent. The depletion layer of the n-ZnO NW surface disappeared almost completely when most of the surface O_2^- molecules became O_2 gas upon exposure to UV light. Figure 11b displays the schematic of the samples placed in the high RH environment with UV light. The surfaces of the p-ZnO:La and n-ZnO NWs were considerably coated with water molecules and a few O_2^- ions; however, the O_2^- ions disappeared quickly under UV exposure. These water molecules form a monolayer under the NW surface and affect conductivity. Recently, some articles have reported the photocatalytic activities of ZnO NSs instead of TiO_2 NSs. The photocatalytic properties of ZnO were improved by doping with La. The photocatalytic properties of the p-ZnO:La NSs produce better reactions than the n-ZnO NSs in aqueous solution.[27,28] The high photocatalytic activities provided more electron and hole exchanges with the water molecules. The photocatalytic layer acts as a conductive path to enhance the photocurrent.

Panels a and b in Figure 12 schematically depict the band diagrams and band edge positions (vs vacuum and normal hydrogen energy level (NHE)) of the p-type ZnO:La and n-ZnO NWs under UV exposure at low and high RH, respectively.[33] Because the ZnO:La NWs is a p-type material, its Fermi level (E_F) was shifted toward the Valence band (E_V). The deep level (E_T) has been related to singly ionized oxygen vacancies and La dopant impurities in the ZnO. This finding suggests that doping impurity dominates the concentration of holes at E_T. The E_F of the n-ZnO NWs was shifted close to the conduction band (E_C). The energy of a 365 nm UV light photon exceeds the band gap of both the p-ZnO:La and n-ZnO NWs, which is around 3.4 eV . Upon exposure to UV (365 nm), the p-ZnO:La and n-ZnO NWs absorbed UV energy, producing many electron−hole pairs. Moreover, excitation by UV light causes electrons to jump to E_C from E_V or E_T.

Figure 12a shows the band diagrams at low RH, where the surface E_F of the p-ZnO:La and n-ZnO NWs shifted toward E_V because the few O_2^- ions increased the concentration of surface holes. The electron concentration of the n-ZnO NW surface was decreased, and then formed a depletion layer. The surface O_2^- ions become O_2 gas upon exposure to UV light; consequently, the electrons were released back to the surface of the NW. These electrons decreased the surface conductivity of the p-ZnO:La NW, but increased it for the n-ZnO NW. Because the E_T of the p-ZnO:La NW contains a large amount of vacancies and dopant, the photo energy was consumed with electrons jumping from E_V to E_T. A few excited electrons jumped directly to E_C from E_V. The characteristic of the p-

dx.doi.org/10.1021/am403364r | ACS Appl. Mater. Interfaces 2013, 5, 11142−11151

ZnO:La NW photoresponse was similar to indirectly band and performance lower I_{UV}/I_{Dark} ratio.

Figure 12b displays band diagrams at high RH, where the water molecules of the NW surface replaced the O_2^- ions. Water molecules covered almost the entire surface of the NW. The O_2^- ions-captured-electrons effect of the p-ZnO:La and n-ZnO has been removed, and so the hole concentration of the NW surface decreased. The E_F of the NW surface shifted toward E_C. The bandgap of the NW absorbed UV photons and generated electron−hole pairs. The activated electrons with an oxidant produced a reduced product, and the generated holes with a reductant produced an oxidized product. Due to the generation of h^+ and e^-, oxidation−reduction reactions take place at the surface of the ZnO, which, in turn, produced free radicals (for example: hydroxyl radicals •OH) able to undergo secondary reactions. In the oxidative reaction, the h^+ reacts with the moisture present on the surface and produces an •OH. Its practical application was made possible by the discovery of water electrolysis by means of TiO_2 or ZnO NSs. The photocatalytic reaction kinetics are as follows[34]

$$ZnO + h\nu \rightarrow ZnO(h^+ + e^-)$$

$$h^+ + H_2O \rightarrow H^+ + \cdot OH$$

$$h^+ + OH^- \rightarrow \cdot OH$$

$$2h^+ + 2H_2O \rightarrow 2H^+ + H_2O_2$$

$$H_2O_{2+}e^- \rightarrow \cdot OH + OH^-$$

The h^+ and e^- are responsible for the production of •OH species, which are formed on the photocatalytic layer and increase the conductivity of water molecules. The photocatalytic layer is only present at the ZnO/water molecule interface. The conductivity of the ZnO:La NWs was increased by ZnO/water molecule photocatalytic efficiency at high RH.

Figure 13 displays the *I*−*V* property of the ZnO:La sample measured under UV exposure at 25 °C in DI water, where the inset schematically displays the *I*−*V* measurement. In DI water, the photocurrent of the ZnO:La sample increased to a maximum of 1.02×10^{-4}A at a 10 V bias. The photocurrent of water compared to 40% RH is around 2 orders. The value of the dark current of water is a minimum of 4.81×10^{-7}A at a 10 V bias. The water I_{UV}/I_{Dark} ratio is around 212.1, which is higher than the 98% RH response. Because water replaced the O_2^- ions and decreased the hole concentration of the p-ZnO:La NW surface, the water dark current of the p-ZnO:La NW was reduced to a minimum. The water dark current of the n-ZnO NW increased due to the removal of O_2^- ions and depletion. In previous articles, the dark current of n-type ZnO NSs was increased almost 10 times at high RH, which induces the low I_{UV}/I_{Dark} ratio.[21,22] The UV response of the n-type ZnO was reduced at high RH, but the p-ZnO:La UV response increased with higher RH.

Panels a and b in Figure 14 display schematics of the UV exposure of p-ZnO:La NWs at low RH and water, respectively. The UV exposure produces the photocatalytic layer at the ZnO/water interface. The photocatalytic layer has an electron channel and high conductivity. The resistance of the p-ZnO:La NWs is very low due to the impedance parallel effect of the photocatalytic layer. The electron conduction path at low RH is shown in Figure 14a. The electrons passed through the surface of the NWs and discontinuous water molecules, which increased conductivity a little. In water, the photocatalytic layer is continuously distributed on the surface of the NWs, as shown in Figure 14b. The conduction paths of the electrons were substantially increased by the photocatalytic layer, which reduced the NW resistance by around 2 orders.

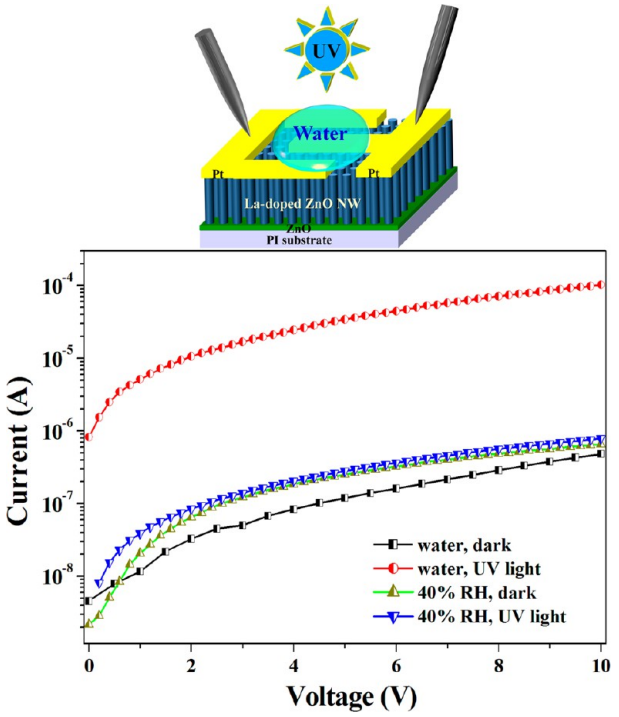

Figure 13. *I*−*V* property of the ZnO:La sample measured under UV exposure in DI water.

CONCLUSION

The high-density ZnO:La NWs uniformly grew hydrothermally on the ZnO/PI substrate. The length and diameter of the NWs were around 860 nm and 80−160 nm, respectively. XRD imaging reveals that all peaks of the La-doped sample shifted to a larger angle, due to the La^{3+} ions preferring interstitial positions in the ZnO lattice, which in turn caused surface oxygen vacancies. The (002) peaks of the ZnO:La NWs shifted about 0.68°. The strong PL peak of the ZnO:La (380 nm) and ZnO NW (378 nm) samples were both close to the 3.3 eV ZnO band edge. PL dominated the ZnO:La NWs with a great amount of oxygen vacancies due to the La impurities. The lattice constants of the ZnO:La NWs (0.514 nm) are smaller than the ZnO (0.522 nm) by HR-TEM. The EDX spectrum determined that the ZnO NWs contain approximately 1.27 atomic% La. The EDX mapping image of the La atoms reveals that La atoms are located in the region of the NWs. The ZnO:La NWs were p-type, as determined by Hall effect measurement. *I*−*V* measurements revealed that nonlinear increases confirmed the favorable Schottky barrier. The dark current of the p-ZnO:La NWs decreased with increased RH. The −68% response of the p-ZnO:La NWs was observed at 98% RH due to the high humidity. The photocurrent of the ZnO:La sample increased with increased RH. The response of 98% RH is around 500%. The I_{UV}/I_{Dark} ratio of 98% RH is around 47.73. The high RH improved the UV PDs response of the p-ZnO:La NWs performance. The photocurrent of water drops compared to 40% RH is around 2 orders. The water I_{UV}/I_{Dark} ratio is around 212.13, whereas the UV PDs response of

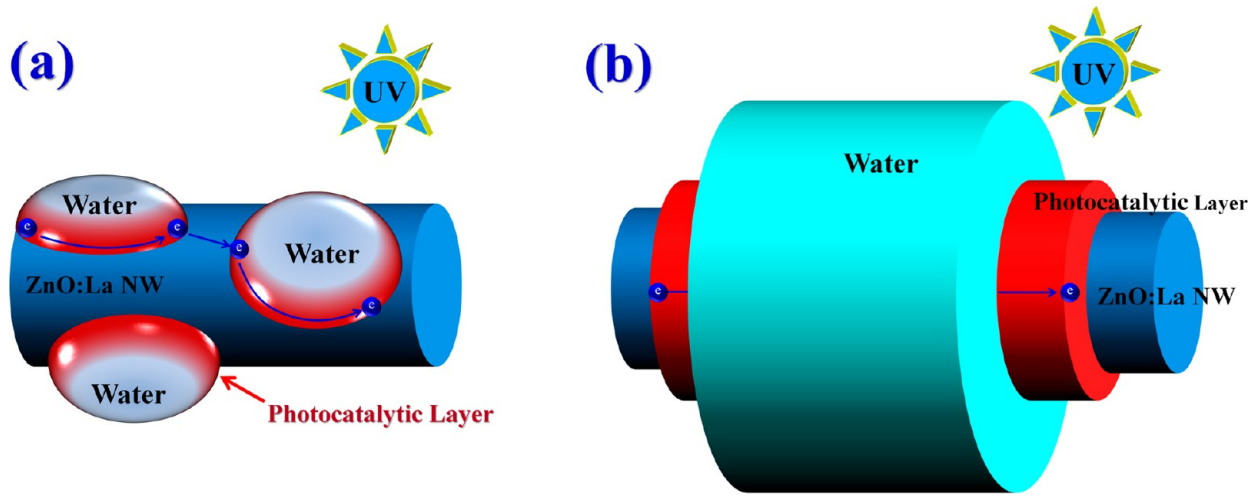

Figure 14. Schematic of UV exposure on the p-ZnO:La NW at (a) low RH; and (b) water.

the p-ZnO:La NWs has the maximum response in DI water measurement.

AUTHOR INFORMATION

Corresponding Authors

*E-mail: clhsu@mail.nutn.edu.tw.

*E-mail: tingjen1123@yahoo.com.tw.

Notes

The authors declare no competing financial interest.

ACKNOWLEDGMENTS

The authors thank the National Science Council of the Republic of China, Taiwan, for financially supporting this research under Contract NSC 102-2221-E-024-017.

REFERENCES

(1) Hsu, C. L.; Lu, Y. C. *Nanoscale* **2012**, *18*, 5710−5717.

(2) Zou, J. P.; Zhang, Q.; Huang, K.; Marzari, N. *J. Phys. Chem. C* **2010**, *114*, 10725−10729.

(3) Hsu, C. L.; Hsueh, T. J.; Chang, S. P. *J. Electrochem. Soc.* **2008**, *155*, K59−K62.

(4) Zheng, M. J.; Zhang, L. D.; Li, G. H.; Zhang, X. Y.; Wang, X. F. *Appl. Phys. Lett.* **2001**, *79*, 839−841.

(5) Hsu, C. L.; Chen, K. C. *J. Phys. Chem. C* **2010**, *116*, 9351−9355.

(6) Vayssieres, L. *Adv. Mater.* **2003**, *15*, 464−466.

(7) Djurisic, A. B.; Leung, Y. H. *Small* **2006**, *2*, 944−961.

(8) Kong, X. Y.; Ding, Y.; Wang, Z. L. *J. Phys. Chem. B* **2004**, *108*, 570−574.

(9) Fang, Y. P.; Pang, Q.; Wen, X. G.; Wang, B. N.; Yang, S. H. *Small* **2006**, *2*, 612−615.

(10) Fan, H. J.; Lee, W.; Hauschild, R.; Alexe, M.; Le Rhun, G.; Scholz, R.; Dadgar, A.; Nielsch, K.; Kalt, H.; Krost, A.; Zacharias, M.; Gosele, U. *Small* **2006**, *2*, 561−568.

(11) Xiu, F. X.; Yang, Z.; Mandalapu, L. J.; Zhao, D. T.; Liu, J. L.; Beyermann, W. P. *Appl. Phys. Lett.* **2005**, *87*, 152101.

(12) Wu, J. J.; Liu, S. C. *Adv. Mater.* **2002**, *14*, 215−218.

(13) Ahn, S. E.; Lee, J. S.; Kim, H.; Kim, S.; Kang, B. H.; Kim, K. H.; Kim, G. T. *Appl. Phys. Lett.* **2004**, *84*, 5022−5024.

(14) Chou, T. H.; Fang, Y. K.; Chiang, Y. T.; Lin, C. I.; Yang, C. Y. *Sens. Actuator A-Phys.* **2008**, *147*, 60−63.

(15) Liao, M. Y.; Koide, Y.; Alvarez, J. *Appl. Phys. Lett.* **2005**, *87*, 022105.

(16) Chen, X. P.; Zhu, H. L.; Cai, J. F.; Wua, Z. Y. *J. Appl. Phys.* **2007**, *102*, 024505.

(17) Wu, H.; Sun, Y.; Lin, D. D.; Zhong, R.; Zhang, C.; Pan, W. *Adv. Mater.* **2009**, *21*, 227−231.

(18) Soci, C.; Zhang, A.; Xiang, B.; Dayeh, S. A.; Aplin, D. P. R.; Park, J.; Bao, X. Y.; Lo, Y. H.; Wang, D. *Nano Lett.* **2007**, *7*, 1003−1009.

(19) Jin, Y. Z.; Wang, J. P.; Sun, B. Q.; Blakesley, J. C.; Greenham, N. C. *Nano Lett.* **2008**, *7*, 1649−1653.

(20) Chen, C. H.; Chang, S. J.; Chang, S. P.; Li, M. J.; Chen, I. C.; Hsueh, T. J.; Hsu, C. L. *Chem. Phys. Lett.* **2009**, *476*, 69−72.

(21) Lai, C. L.; Wang, X. X.; Zhao, Y.; Fong, H.; Zhu, Z. T. *RSC Adv.* **2013**, *3*, 6640−6645.

(22) Li, Y. B.; Della Valle, F.; Simonnet, M.; Yamada, I.; Delaunay, J. J. *Appl. Phys. Lett.* **2009**, *94*, 023110.

(23) Hsueh, H. T.; Hsueh, T. J.; Chang, S. J.; Hung, F. Y.; Tsai, T. Y.; Weng, W. Y.; Hsu, C. L.; Dai, B. T. *Sens. Actuators, B* **2011**, *156*, 906−911.

(24) Yang, X. Y.; Wolcott, A.; Wang, G. M.; Sobo, A.; Fitzmorris, R. C.; Qian, F.; Zhang, J. Z.; Li, Y. *Nano Lett.* **2009**, *9*, 2331−2336.

(25) Shan, C. X.; Liu, Z.; Hark, S. K. *Appl. Phys. Lett.* **2008**, *92*, 073103.

(26) Sun, M. H.; Zhang, Q. F.; Wu, J. L. *J. Phys. D: Appl. Phys.* **2007**, *40*, 3798−3802.

(27) Suwanboon, S.; Amornpitoksuk, P.; Sukolrat, A.; Muensit, N. *Ceram. Int.* **2013**, *39*, 2811−2819.

(28) Anandan, S.; Vinu, A.; Lovely, K. L. P. S.; Gokulakrishnan, N.; Srinivasu, P.; Mori, T.; Murugesan, V.; Sivamurugan, V.; Ariga, K. *J. Mol. Catal. A: Chem.* **2007**, *266*, 149−157.

(29) Khatamian, M.; Khandar, A. A.; Divband, B.; Haghighi, M.; Ebrahimiasl, S. *J. Mol. Catal. A: Chem.* **2012**, *365*, 120−127.

(30) Lyu, S. C.; Zhang, Y.; Ruh, H.; Lee, H. J.; Shim, H. W.; Suh, E. K.; Lee, C. J. *Chem. Phys. Lett.* **2002**, *363*, 134−138.

(31) Barsan, N.; Schweizer-Berberich, M.; Gopel, W. *Fresenius J. Anal. Chem.* **1999**, *365*, 287−304.

(32) Hsu, C. L.; Chen, K. C.; Tsai, T. Y.; Hsueh, T. J. *Sens. Actuators, B* **2013**, *182*, 190−196.

(33) Zhu, H. M.; Lian, T. Q. *Energy Environ. Sci.* **2012**, *5*, 9406−9418.

(34) Daneshvar, N.; Salari, D.; Khataee, A. R. *J. Photochem. Photobiol., A* **2003**, *157*, 111−116.